

Flexible and Printed Electronics



PAPER

Improvements in the electromechanical properties of stretchable interconnects by locally tuning the stiffness

RECEIVED

8 November 2019

REVISED

29 November 2019

ACCEPTED FOR PUBLICATION

7 January 2020

PUBLISHED

23 January 2020

Milad Mosallaei , **Donato Di Vito** , **Behnam Khorramdel**  and **Matti Mäntysalo** 

Faculty of Information Technology and Communication, Tampere University, Tampere, Finland

E-mail: milad.mosallaei@tuni.fi**Keywords:** stretchable electronics, printed electronics, screen-printing, finite element (FE) analysis, electromechanical properties, strain concentration, stress distribution

Abstract

Recent advances in materials science and structural design have changed electronic applications from being bulky and rigid objects to small and soft products that have emerged for a wide range of applications, especially human-related products for which mechanical adoption is the key requirement. A typical stretchable application consists of small-sized, rigid IC-chips and passive components interconnected by conductive tracks on soft substrates. The early failure of such devices initiates from the rigid-soft interface due to the accumulation of stress. Therefore, special attention is needed to reduce the strain concentration at the interface. In this paper, stretchable interconnects were fabricated using a screen-printing method and surface mounted devices (SMDs) were bonded using an isotropic conductive adhesive. By partially removing material from the substrate in areas a little way from the rigid components, the stiffness is locally reduced, and this leads to an increase in the local stiffness around the SMDs and hence shields the soft-rigid interface against the stress. Materials can be removed by two different patterns. A finite element analysis and experimental data show 11%–19% improvements in single pull-up tests for the modified samples. This approach makes the electromechanical behaviour independent of encapsulation properties.

1. Introduction

Conventionally, electronic applications refer to combinations of rigid active units that are densely packed together on hard and brittle substrates. Unlike the high reliability, availability, technology maturity and life span of these devices, it is not feasible to use them in certain applications where mechanical flexibility is key, such as for electronic skin (E-skin) [1, 2]. For this reason, researchers are trying to develop deformable electronics. Soft electronic applications would allow the benefits from traditional rigid systems and the freedom of design in deformable electronics to be combined [3, 4]. This unique ability can be widely employed through potential applications in wearable electronics [5], healthcare [6], consumer electronics, conformable displays, electrocardiogram/ electroencephalogram (ECG/EEG) monitoring [7], human body temperature measurement systems [8], and sweat analysis units [9]. The main challenge in stretchable electronics is to achieve high performing

electronic functionality for an elastic and low modulus system [10]. An essential requirements for fabricating deformable devices is the development of new classes of materials which are compatible with deformation, mechanical design, and fabrication techniques [3, 6, 11, 12].

Due to the low intrinsic capability of conventional conductive materials (e.g. silver) to resist strain, one way to increase their mechanical deformability is to prepare a composite system of conductive particles into a matrix of polymeric materials and a solvent. Metal nanowires (NWs), carbon nanotubes (CNTs), conductive polymers and metal nanoparticles (NPs) are all examples of stretchable conductors [13, 14].

Elastomeric polymers such as ethylene propylene diene monomer rubber (EPDM), polyurethane (PU) and polydimethylsiloxane (PDMS) are common stretchable substrates due to their compliant mechanical properties, availability and ease of processability [15–17]. However, EPDM and PDMS have inherent hydrophobic nature (unlike PU) that requires surface

Table 1. Properties of substrate and conductive material used in FE analysis.

TPU properties			Conductive paste properties	
i	μ_i	α_i	E (GPa)	1.725
1	-4.725	1.402	ν	0.3
2	1.392	3.295	Yield stress 1 (MPa)	19.67 at $\varepsilon_p = 0$
3	9.196	-2.075	Yield stress 1 (MPa)	24.35 at $\varepsilon_p = 0.0698$

treatment (e.g. oxygen plasma treatment) prior to deposition of functional inks to improve the adhesion between the ink and the substrate [18, 19].

Structural design to combine different materials with considerable differences in mechanical and physical properties plays a crucial role in stretchable electronics [3, 20]. In a common approach, miniaturized, rigid, functional units are interconnected by either geometrically engineered or intrinsically stretchable interconnects (the island-bridge technique) [14, 21].

In the work described, e.g. in [22–25], the electro-mechanical properties of devices were improved by adding encapsulant/support materials. This approach, distributes the plastic strain over a wider area where it reduces the local strain concentration. This mechanical improvement successfully enhances the electrical properties during the deformation.

In this paper, we propose a method to reduce the strain concentration in close proximity of the rigid-soft interfaces by partially removing material. To achieve this, we studied passive surface mounted devices (SMDs) mounted with isotropic conductive ink (ICA) on a screen-printed stretchable circuit board. Rigid-soft interfaces (i.e. SMD-interconnections) have a high stress-strain concentration when the system is stretched, which then become starting locations for a failure. We designed and optimized two geometries using a finite element (FE) analysis. Samples were fabricated with a reference sample to demonstrate the improvements.

2. Finite element analyses

The mechanical behaviour of the samples was analysed using the commercial finite element software ABAQUS CAE. Each model consisted of three different parts, which were assembled using tie constraint conditions. In particular, the SMD was modelled as a discrete rigid form since its mechanical stiffness is very high compared to the underlying components. The thermoplastic polyurethane (TPU) substrate was modeled as an incompressible hyper-elastic material following Ogden's model with $N = 3$ [26]. The conductive track, instead, were modelled as a linear elastic material with two yield points and a perfectly plastic behaviour after the second yield point. The

properties used to describe the behaviour are shown in table 1.

The properties for the substrate were obtained by fitting of the uniaxial tensile behaviour of a pure substrate sample. The properties for the conductive ink, instead, were gathered by testing a conductive film supported on a TPU substrate layer, as previously done in the works by [27, 28]. The characteristic size of the elements in the model were 0.125 mm for the conductive track and 0.250 mm for the substrate, while the elements used were C3D8 and C3D8H, respectively. The exact part geometry used in the FE models and the applied loading conditions are shown in table 1. These boundary conditions correspond to a uniaxial tensile load up to a nominal strain (defined as the change in length of the sample over its original length, $\varepsilon = \Delta L/L_0$) of 0.4 of the sample original length, i.e. up to a stretch ratio of 1.4.

The geometries chosen for the substrate were optimized through an FE analysis to determine the effect of their geometrical features on the conductive track deformation behaviour. The updated versions of the geometries were analysed under the same loading conditions as the standard geometries, as shown in figure 1.

3. Materials and fabrication

We used a 50 μm thick TPU, U4201 provided by Epurex Platilon as the stretchable substrate. High dielectric properties, high elasticity and high stretchability before failure (300%) are among the properties of this film. On the other hand, this material shows hysteresis at high levels of deformation, which suggests that from a modelling point of view, the material can be considered as a purely hyper-elastic material only for quasi-static loading. For the fabrication of conductive tracks, a commercially available conductive silver flake paste (CI-1036) from engineered conductive materials (ECM) was employed. The total solid content of this conductive paste is 66%, and the viscosity and the density are 10 000 mPa s at 25 C and 2.08 kg l⁻¹, respectively. The size of silver flakes in this ink is between 7 μm and 10 μm [27]. The curing temperature of the silver paste (125 °C) is lower than the softening temperature range of TPU (155–185 °C) and this makes it feasible to cure the paste on the substrate. To mimic the rigid islands on the substrate, zero-ohm resistors were used as SMDs. For this aim, we employed an SMD 2512 with the physical dimensions of 6.3 mm \times 3.2 mm from TopLine Corporation. The standard pad size for this SMD component is 8.1 mm \times 3.5 mm. An ICA from Namics (XE184A) was used to bond the SMD to the substrate. This ICA has high flexibility and a low modulus (0.25 GPa) compared to similar ICAs. It has solid content about 75% and the mean value for the filler size is 12 μm where the maximum filler size reaches 65 μm . The

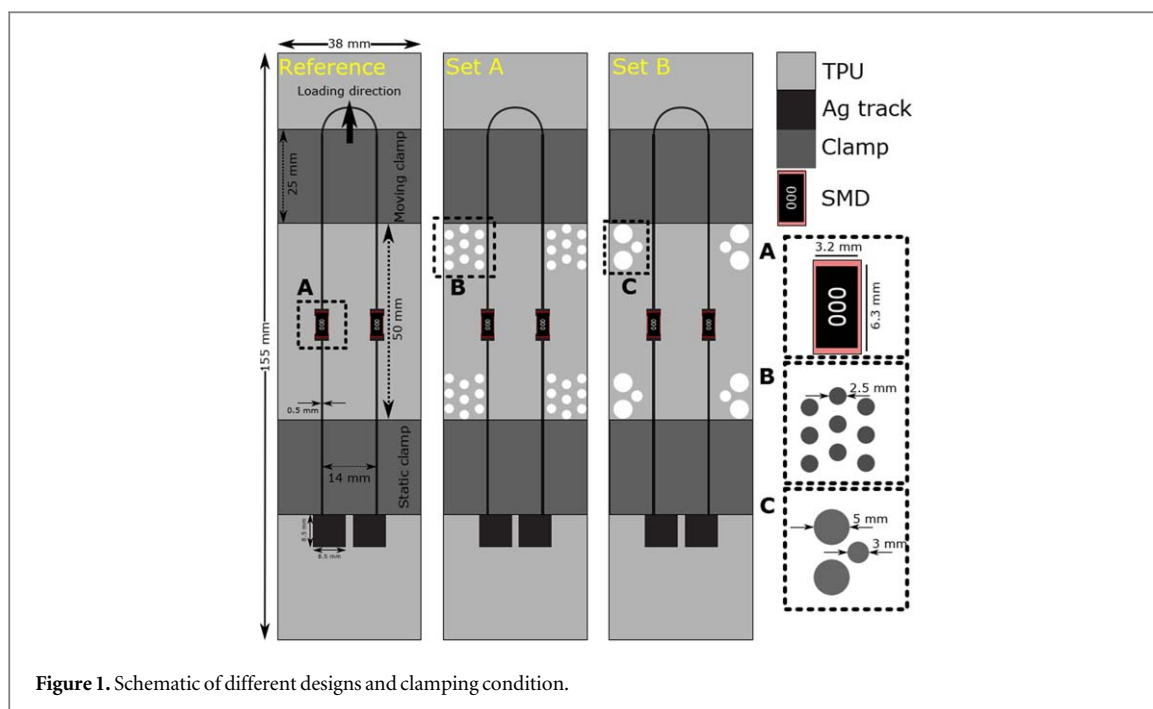


Figure 1. Schematic of different designs and clamping condition.

viscosity of the ICA is 30 Pa s at 25 °C. The volume resistivity and adhesion strength of the ICA are and 1.5 N mm^{-2} respectively. A pressure sensitive adhesive transfer tape from 3 M (Tape 9703) were used to make electrical connection and physical bonding between the Keithley probes and the interconnects pads during the stretching test.

The following procedure describes the fabrication steps of the stretchable interconnects:

1. Slight stretching of the TPU sheets (nominal stain of 0.03–0.05) and then attachment on 2 mm thick aluminum plates.
2. Screen printing of the conductive paste by a semi-automatic screen printer from TIC (SCF-300) in two printing cycles.
3. Annealing of the samples at 125 °C for 30 min in an oven for curing of the conductive track.
4. Dispensing ICA and mounting SMD components.
5. Curing of ICA in an oven at 100 °C for 30 min.

The final stage before the reliability tests is to cut the samples into defined template and remove the material from the substrate in desired shapes. To achieve the desired precision of the final samples, a laser cutter (Trotec Speedy 100) was employed. The laser intensity and cutting speed were adjusted accordingly based on the substrate.

4. Characterization and reliability methods

After the fabrication of the samples, they were observed with an optical microscope to ensure the absence of visible defects in the conductive tracks. A batch of 10 samples from each set, were unidirectionally pulled up by a tensile tester (Instron 4411 universal Testing Machine) to the point where the conductance went to zero. A dedicated clamping system with a thin layer of rubber was used to ensure a tight grip on the samples during the stretching. To avoid damaging the conductive tracks caused by the clamps, grooves were created on the rubber surfaces. In this configuration, pads of samples were located below the fixed clamps to eliminate the measurement noise during the electro-mechanical experiments. A 500 N load cell was used to stretch the samples with a grip speed of 6 mm min^{-1} . The DC resistances of the samples were simultaneously measured using a Keithley 2425 multimeter with a sample rate of 5 Hz, which was triggered by customized software written in LabVIEW. The detailed information of the test set-up can be seen in [27, 29].

To simulate the real-life conditions of the devices under persistent mechanical loads, we investigated the change in the electrical behaviour of the samples under a constant load applied to the samples (creep test) and constant displacement (stress relaxation). A load of 3 N was used as a set point for the creep test. All sets of samples were pulled up accordingly and kept for 120 min after reaching to the set point. The changes in length and resistance of the samples were recorded accordingly. In order to perform stress relaxation experiments, a tensile nominal strain of 0.2 was imposed on the samples for 120 min.

Successive cyclic tests were also conducted to study the durability under dynamic loading/unloading condition. For this reason, the samples were tested by stretching to a maximum nominal strain of 0.2 and at a cyclic speed of 200 mm min^{-1} .

Scanning electron microscope (SEM) imaging was carried out using a Tescan Vega SEM to study the quality of interfaces between the SMD/ICA and ICA/conductive lines. Prior to the SEM imaging, the samples were coated with a thin layer of carbon using Agar Turbo Carbon Coater to avoid charging the sample during the SEM imaging.

The deformation behaviour of different samples was also analysed using a digital image correlation (DIC) system. For this purpose, a black speckle pattern was sprayed on the samples surface using a water-based paint, after evaluating that the particles would not have any effect on the mechanical behaviour of the sample. The speckles had an approximate dimension of $50 \mu\text{m}$ and a negligible thickness. The images were taken with a SONY $\alpha 5000$ with a CMOS RGB 20MP sensor (with a raw image resolution equal to 5496×3656 pixels) equipped with a 30 mm F/2.8 objective lens. The samples were then clamped on the tensile tester and images were taken every 2.5 mm of crosshead displacement, up to a total imposed displacement of 20 mm (equal, for the tested sample, to a stretch ratio of 1.4). The resulting images were analysed using the commercial software DAVIS 10 to get information about the deformation fields along the conductive tracks and, in general about the deformed samples.

5. Results and discussion

Several FE analyses were used to identify the conductive track behaviour, the highest deformation levels achieved on the tracks and their location. These notions were used to better understand the influence of each design on the electrical response happening upon deformation.

The results of the FEA are shown in figure 2. The plots representing the true strain at the maximum displacement imposed on the samples are shown in figure 2(A). Here it is possible to notice how the highest deformation levels on the track vary strongly based on the geometry of the removed areas. This difference in deformation behaviour arises from the different geometry of the two samples, even though the amount of material removal is similar (44 mm^2 for the Set A and 46 mm^2 for the Set B). This difference is justified by the proximity of the removed shapes to the tracks for Set A. This feature varies strongly with the amount of material removed from the sample, and the FE sensitivity analyses highlighted different kinds of behaviour for different feature sizes, as shown in figures 2(B), (C).

It is possible to notice that for shapes smaller than 0.5 mm in radius the effect on the track deformation behaviour is negligible since the geometrical features are too small to affect the deformation of the samples. However, the deformation behaviour starts to be predominant with respect to the presence of the SMD for shapes bigger than 1 mm in radius. A similar behaviour is also recognizable in the Set B design with slightly different feature sizes.

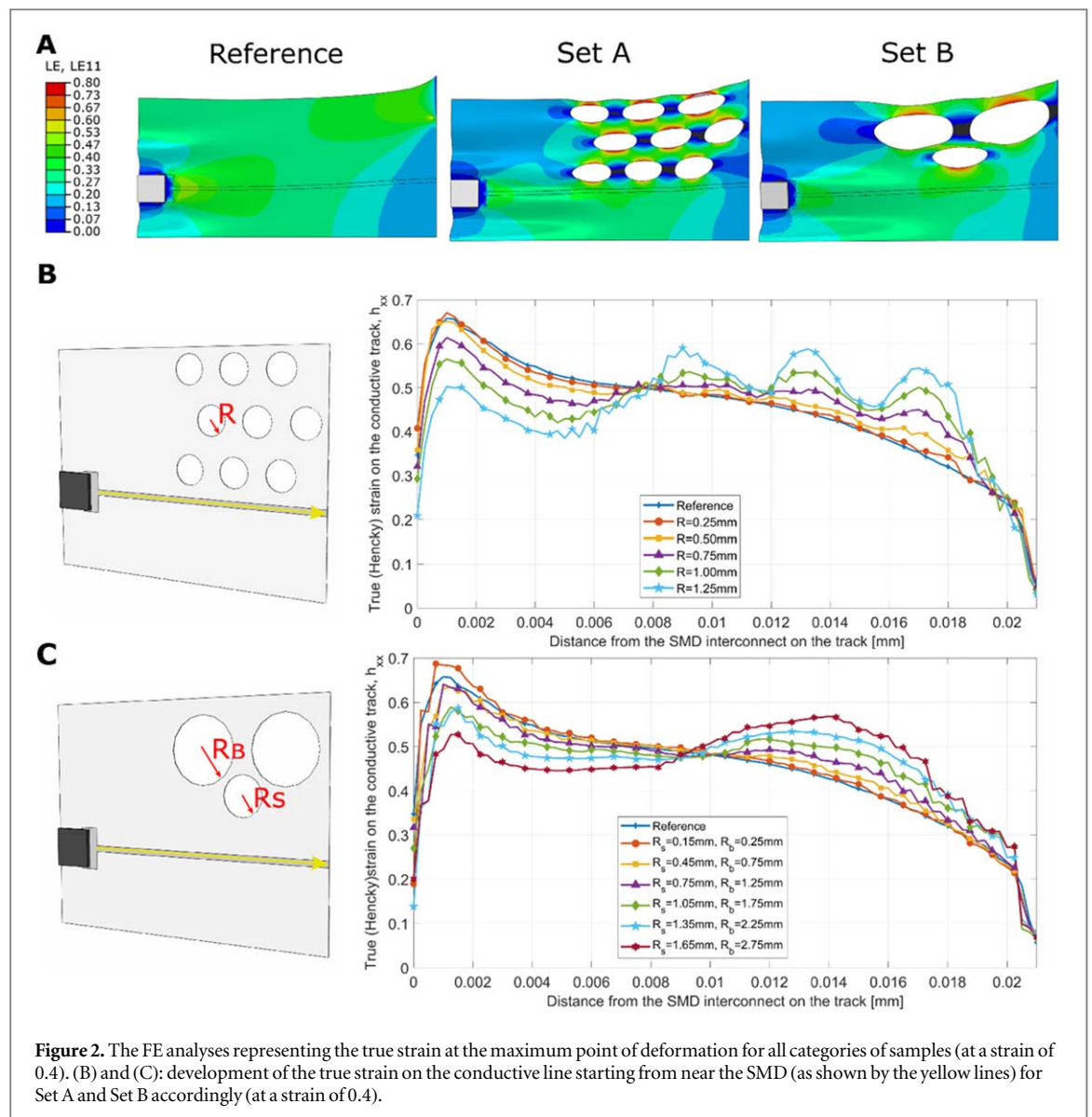
The performed sensitivity analyses show that both the presence of the SMD and the material removed have different influences on the deformation behaviour of the systems analysed. By tuning the geometrical parameters of the removed materials, it is possible to induce strain concentrations in either part of the stretchable sample, and for a specific range of such parameters it is possible to even out the strain distribution along the conductive tracks.

By choosing the geometrical parameters within the said windows, it is possible to minimize the deformation peaks on the conductive tracks and consequently this achieve better expected behaviour for the whole sample under static loading. Based on the FE sensitivity analyses, sample Set A with $R = 1.25 \text{ mm}$ and Set B with $R_S = 1.5 \text{ mm}$ and $R_B = 2.5 \text{ mm}$ was fabricated for experimental characterization.

The performed DIC tests on different designs show a good agreement with the FE results shown in figure 2(A). In fact, the strain peaks reached on the sample tend to be very close to each other at various different deformations. In particular, the peaks of the deformation reached by imposing an overall stretch ratio of 1.7 on sample Set B were equal to 0.58 in the FE analysis and equal to 0.57 in the DIC results. These analyses allowed us to better understand the behaviour of the tested samples and to more easily localize the peaks of deformation on the different samples.

Figure 3(A) shows a comparison of the deformation fields for the three different analysed shapes, highlighting the deformation peaks that occur due to the presence of the circular holes. As can be seen, the main effect of these geometries during loading are the strain concentrations formed in these specific locations of the sample. However, the distance of the holes from the tracks greatly influences the conductive track behaviour: when employing the Set A geometry it is possible to notice that the strain concentration strongly influences the deformation behaviour of the tracks themselves, leading to peaks of deformation that can be even higher than the strain concentration near the SMD-conductive track edge.

In order to more quantitatively compare the differences in the deformation behaviour between the different designs, figure 3(B) shows the computed strains over the different tracks at an imposed stretch ratio of 1.4. The maximum deformation reached on the conductive tracks for the reference, Set A and Set B is equal to 0.51, 0.42 and 0.38, respectively. As also mentioned before, the said value was reached near the



SMD-conductive track edge for both the reference and for Set B, while for Set A the peak deformation was reached near the circular holes. Consequently, this is also the expected electromechanical failure point for this specific design.

Figure 4 summarizes the result of single pull-up test for different sets of samples. As it can be seen, sample Set A and Set B have average stretchability with a nominal strain of 0.36 and 0.44 that are better performances in comparison with the reference sample (0.25). In the reference sample, the strain localizes around the components because of their presence on the substrate. In fact, the reaction force exerted by these rigid components on the substrate induces the strain localization around them and prevents the homogenous distribution of deformations throughout the sample. Additionally, the presence of edges and interfaces of the conductive tracks and ICAs tended to intensify these effects. This, in turn, influenced microcrack nucleation on the conductive line upon deformation due to local concentration of strains in

the polymeric binder of the conductive track, which reached and overcame the yield point during loading. Thus, these materials were intended to form microcracks to relieve the strain in response to higher deformation values. After the nucleation of microcracks, however, steady crack growth took place during further stretching until the electromechanical failure of the track, which occurred by the formation of major fractures in the conductive lines. However, in sample Set A and Set B, the increase of the stiffness around the rigid component reduced the strain concentration in this area compared to the reference sample. On the other hand, lowering the stiffness (by removing material) in regions away from the SMDs, which can sustain higher load levels, resulted in higher stretchability. The reason for choosing circles over other shapes (rectangles, ovals, etc) for removing the materials, was to avoid sharp corners that would act as stress concentrators.

These circles, generate strain concentrations away from the conductive tracks as they act as

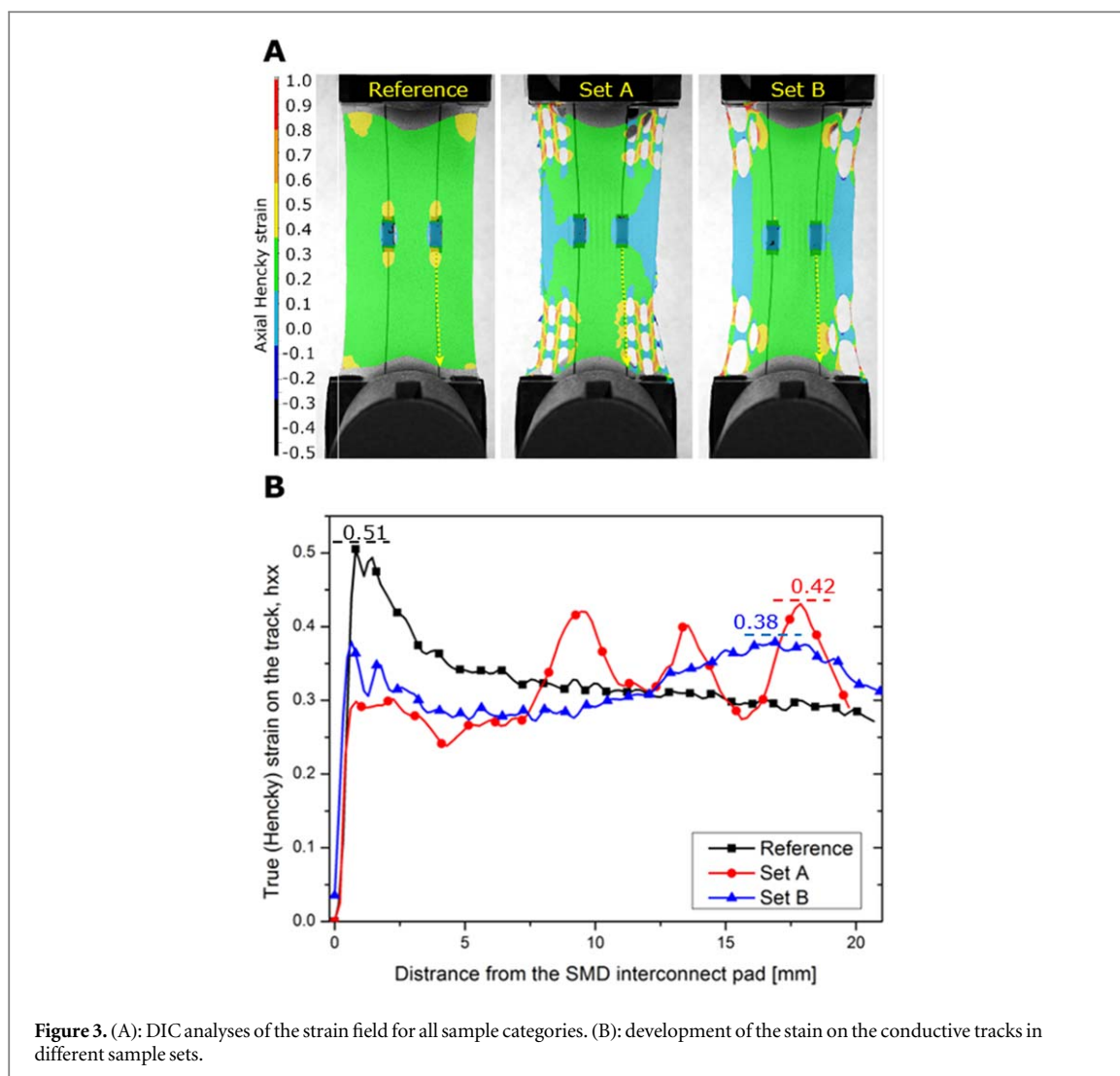


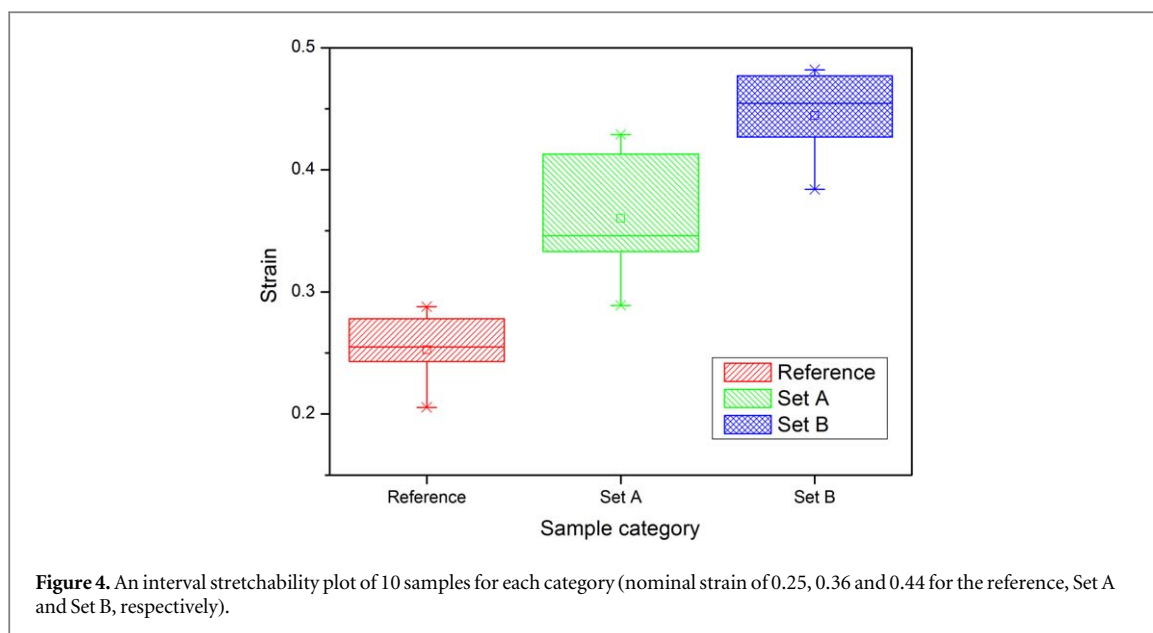
Figure 3. (A): DIC analyses of the strain field for all sample categories. (B): development of the stain on the conductive tracks in different sample sets.

discontinuities on the substrate. However, they were away than conductive lines where the electrical conductivity was not affected. Although this approach cannot eliminate all the strain concentration around the rigid components, it can reduce the value and hence slow the nucleation of microcracks and reduce their density in critical regions of the sample. In connection with this, figure 5 shows optical microscope images of the area next to the component's pad for all three samples at a nominal strain of 0.2. It can be clearly seen that the density of the microcracks is different in the three designs, as expected from the preliminary analyses performed.

During the creep test, the minimum amount of deformation (6.7 mm) happened for the reference sample when it was unidirectionally stretched up by force of 3 N. Similarly, the normalized resistance (resistance after 120 min/resistance at the moment the sample is stretched by a force of 3 N) was 1.7 for this sample since it was stretched less in comparison to the other modified samples. The normalized resistances for Set A and Set B are 5.0 and 5.3 accordingly. Figure 6 summarizes the deformation of all samples during 120 min under constant load of 3 N. As the

surface area is greater in the reference sample compared to the other samples, a larger force is required for the same deformation than for the other two samples. In this experiment, the force was kept constant for all samples and therefore less deformation happened to the reference sample in identical experiments, since this sample showed an overall higher level of stiffness. In addition, sample Set A and Set B were able to deform more at a fixed level of force (even over time) compared to the reference sample. They were also less obtrusive and could be preferable when using them in health/fitness sensing applications.

In a relaxation experiment, all samples kept their conductivity during the test. Figure 7 shows the change in resistances for all samples over 120 min. Resistances of the reference sample, Set A and Set B decreased to 88.2%, 91.0% and 97.7% of their maximum resistance at the beginning of the stress relaxation tests. It can be concluded that since in the reference sample we did not remove any part from the substrate, the entire sample relaxed in a more uniform way than other modified samples and hence resulted in a larger drop in resistance.



During the cyclic fatigue test, the modified samples failed at a higher number of cycles (105, 173 and 227 cycles for the reference, Set A and Set B respectively). In these loading configurations, the durability of the samples depends not only on the nucleation and growth of microcracks, but also on interfacial delamination. When the device is under frequent loading, cracks develop in stiffer material and debonding can occur in the interfacial layers. While the conductive tracks remained unchanged when samples were relaxed, a few microcracks formed upon stretching with a strain of 0.2 (as already shown in figure 5). However, these microcracks could grow and join upon additional cycles. To improve the reliability under cyclic loading, using wider conductive lines is suggested where the microcracks can distribute over a larger area.

Figure 8(A) is a schematic of the cross section of the device explaining the interfaces between different parts. Figure 8(B) shows an SEM image of a fresh device without a deforming history and figure 8(C) demonstrates a sample that experienced 1000 cycles at a strain of 0.2. All images were taken in the relaxed condition. At the same time, the bonding between the SMD and ICA remained quite robust even after 1000 cycles, while the interface between the ICA and the conductive lines was deformed. While this region is intact for the fresh sample, the ICA slipped and debonded from the conductive line for the sample experienced the cyclic loading. The mechanical mismatching properties cause stress on the interface and by suffering from poor adhesion, debonding occurs accordingly. This phenomenon happened for all the samples in an identical manner. However, the intensity was greater for the reference sample. Since the mechanical properties of the ICA and conductive line are different, it leads them to behave differently against the deformation. To reduce the mechanical mismatch between

the ICA and conductive materials, the authors suggest using ICAs with a lower Young's modulus in future studies.

6. Summary and conclusion

A typical stretchable device combines different materials with significant differences in physical and mechanical properties. In a common approach to link miniaturized functional units with stretchable interconnects on elastic substrates. The interface between the rigid and soft materials prevents the even distribution of stress over the media and thus concentrates the strain that leads to early failure of the device.

In this paper, the strain concentration at the interface of rigid-soft components was mitigated by locally tuning the substrate. More precisely, two sets of samples were designed by partially removing the substrate in areas far away from the rigid components. This modification increased the stiffness around the SMDs in order to homogenize the strain field along the conductive track, thus avoiding strain concentrations near the components. Furthermore, an FE analysis and experimental results showed that not only removing the material but also the shape and density of the removal materials could affect the strain distribution of the sample. We also used DIC analyses to prove our hypothesis and highlight the strong differences in strain fields among the chosen designs. This modification resulted in better electromechanical behaviour under different loading types, i.e. quasi-static and cyclic loading, creep and stress relaxation. Local tuning of the stiffness can be done also by means of encapsulation. However, encapsulation requires an extra stage in the fabrication process that is not economically and environmentally beneficial. In addition, the electromechanical properties of the samples would be dependent on the encapsulant properties.

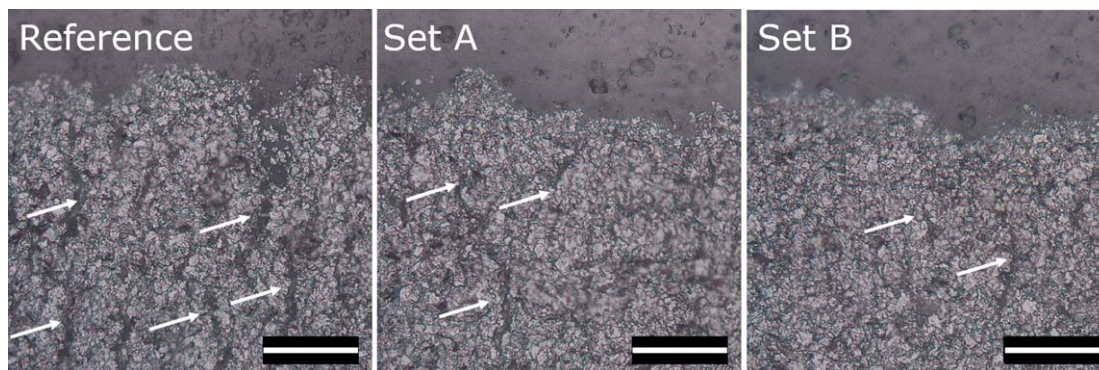


Figure 5. Optical microscope images of different samples stretched by a strain of 0.2 (next to the SMD). Scale bar: 100 μm . Arrows mark some of the emerged microcracks on the conductive lines.

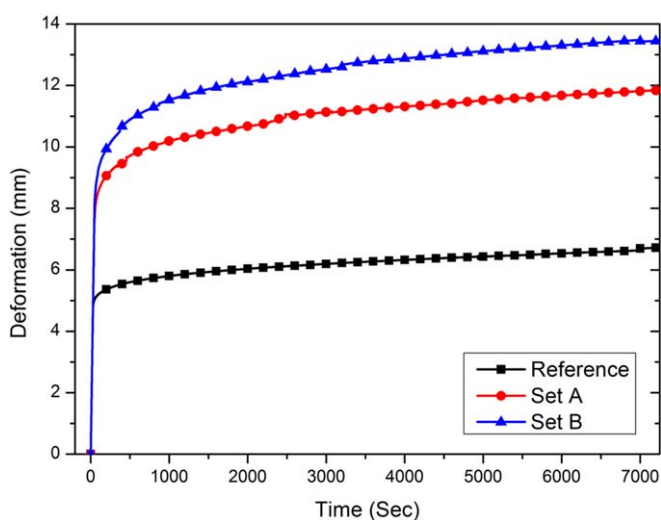


Figure 6. Deformation of different samples during the creep test (constant load for 120 min).

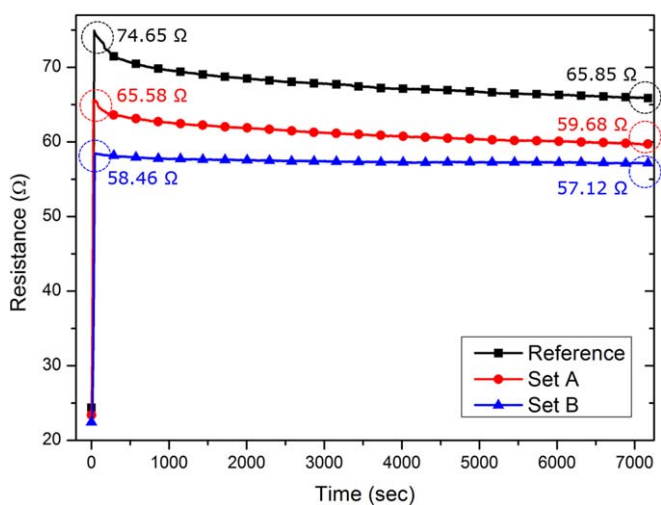
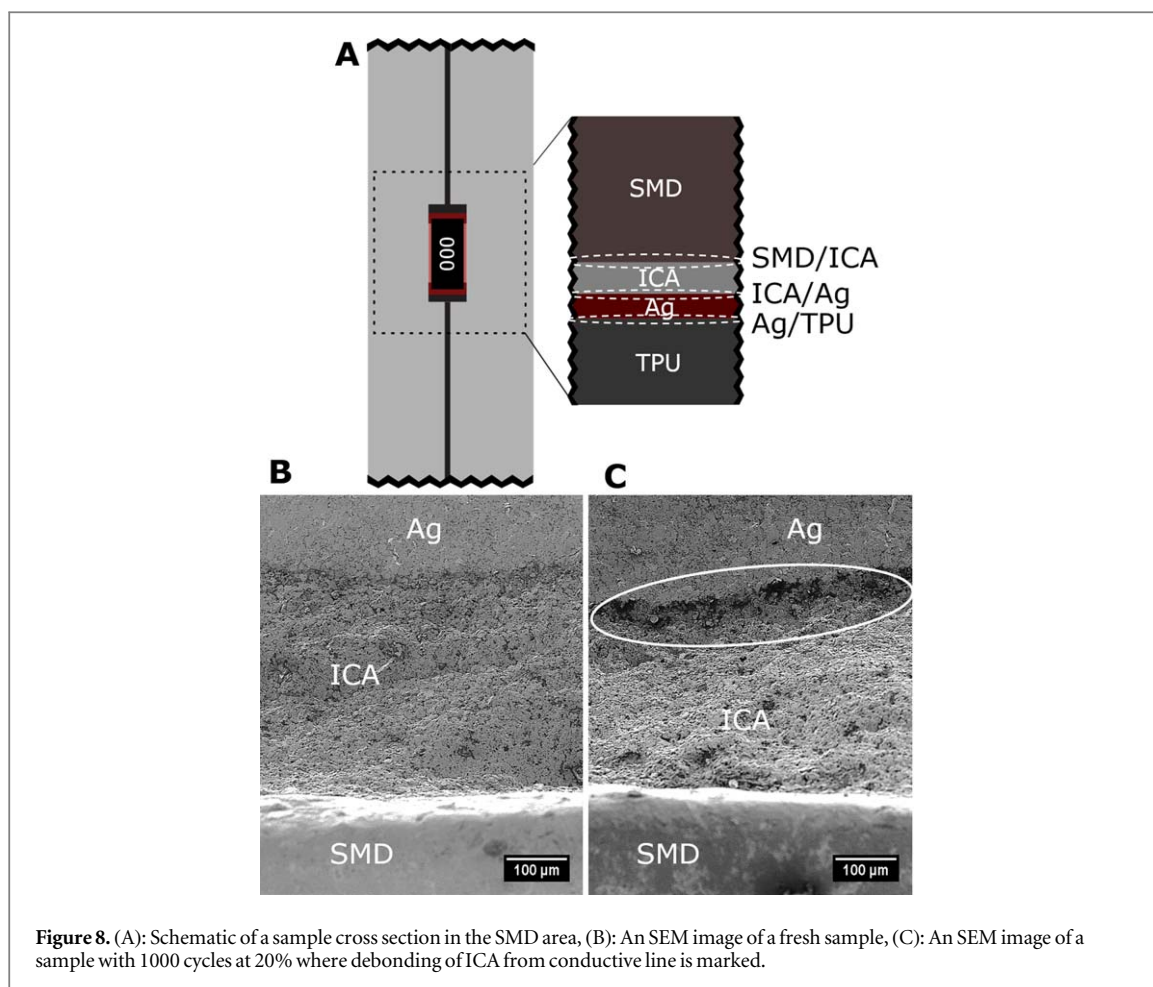


Figure 7. Comparison of change in resistance of different samples during the relaxation test.



Acknowledgments

This work is funded by Business Finland (Grant No: 2947/31/2018) and Academy of Finland (Grant project No: 292477). M Mäntysalo is supported by Academy of Finland (Grant No: 288945). This project utilized the ‘Printed Intelligence Infrastructure’ (PII-FIRI, Grant No: 320019).

This work made use of Tampere Microscopy Center facilities at Tampere University. The authors also wish to acknowledge CSC—IT Centre for Science, Finland, for computational resources.

ORCID iDs

Milad Mosallaei  <https://orcid.org/0000-0003-1461-0961>

Donato Di Vito  <https://orcid.org/0000-0003-0602-9288>

Behnam Khorramdel  <https://orcid.org/0000-0001-6411-9228>

Matti Mäntysalo  <https://orcid.org/0000-0002-7780-6454>

References

- [1] Lu Y, Biswas M C, Guo Z, Jeon J-W and Wujcik E K 2019 Recent developments in bio-monitoring via advanced polymer nanocomposite-based wearable strain sensors *Biosens. Bioelectron.* **123** 167–77
- [2] Ray T *et al* 2019 Soft, skin-interfaced wearable systems for sports science and analytics *Curr. Opin. Biomed. Eng.* **9** 47–56
- [3] Dang W, Vinciguerra V, Lorenzelli L and Dahiya R 2017 Printable stretchable interconnects *Flex. Print. Electron.* **2** 013003
- [4] Harris K D, Elias A L and Chung H-J 2016 Flexible electronics under strain: a review of mechanical characterization and durability enhancement strategies *J. Mater. Sci.* **51** 2771–805
- [5] Yokus M A, Foote R and Jur J S 2016 Printed stretchable interconnects for smart garments: design, fabrication, and characterization *IEEE Sens. J.* **16** 7967–76
- [6] Do T N and Visell Y 2017 Stretchable, twisted conductive microtubules for wearable computing, robotics, electronics, and healthcare *Sci. Rep.* **7** 1753
- [7] Stauffer F *et al* 2018 Skin conformal polymer electrodes for clinical ECG and EEG recordings *Adv. Healthc. Mater.* **7** 1700994
- [8] Chen Y, Lu B, Chen Y and Feng X 2015 Breathable and stretchable temperature sensors inspired by skin *Sci. Rep.* **5** 11505
- [9] Choi J, Ghaffari R, Baker L B and Rogers J A 2018 Skin-interfaced systems for sweat collection and analytics *Sci. Adv.* **4** eaar3921
- [10] Fan J A *et al* 2014 Fractal design concepts for stretchable electronics *Nat. Commun.* **5** 3266
- [11] Tao X, Koncar V, Huang T-H, Shen C-L, Ko Y-C and Jou G-T 2017 How to make reliable, washable, and wearable textronic devices *Sensors* **17** 673

- [12] Reeder J T *et al* 2019 Waterproof, electronics-enabled, epidermal microfluidic devices for sweat collection, biomarker analysis, and thermography in aquatic settings *Sci. Adv.* **5** eaau6356
- [13] Nagels S and Deferme W 2018 Fabrication approaches to interconnect based devices for stretchable electronics: a review *Materials* **11** 375
- [14] Yang J C, Mun J, Kwon S Y, Park S, Bao Z and Park S 2019 Electronic skin: recent progress and future prospects for skin-attachable devices for health monitoring, robotics, and prosthetics *Adv. Mater.* **31** 1904765
- [15] Noh J-S 2016 Conductive elastomers for stretchable electronics, sensors and energy harvesters *Polymers* **8** 123
- [16] Cataldi P *et al* 2018 Carbon nanofiber versus graphene-based stretchable capacitive touch sensors for artificial electronic skin *Adv. Sci.* **5** 1700587
- [17] Wang Y, Li Z and Xiao J 2016 Stretchable thin film materials: fabrication, application, and mechanics *J. Electron. Packag.* **138** 020801
- [18] Moraes J H *et al* 2007 Surface improvement of EPDM rubber by plasma treatment *J. Phys. D: Appl. Phys.* **40** 7747–52
- [19] Trantidou T, Elani Y, Parsons E and Ces O 2017 Hydrophilic surface modification of PDMS for droplet microfluidics using a simple, quick, and robust method via PVA deposition *Microsyst. Nanoeng.* **3** 16091
- [20] Gonzalez M, Axisa F, Vanden Bulcke M, Brosteaux D, Vandeveldel B and Vanfleteren J 2008 Design of metal interconnects for stretchable electronic circuits *Microelectron. Reliab.* **48** 825–32
- [21] Zhang Y *et al* 2013 Buckling in serpentine microstructures and applications in elastomer-supported ultra-stretchable electronics with high areal coverage *Soft Matter* **9** 8062
- [22] Wu J *et al* 2011 Stretchability of encapsulated electronics *Appl. Phys. Lett.* **99** 061911
- [23] Li K *et al* 2019 A generic soft encapsulation strategy for stretchable electronics *Adv. Funct. Mater.* **29** 1806630
- [24] Bossuyt F, Vervust T and Vanfleteren J 2013 Stretchable electronics technology for large area applications: fabrication and mechanical characterization *IEEE Trans. Components, Packag. Manuf. Technol.* **3** 229–35
- [25] Loher T *et al* 2009 Stretchable electronic systems: realization and applications 2009 11th Electronics Packaging Technology Conf. pp 893–8
- [26] Ogden R W 1972 Large deformation isotropic elasticity—on the correlation of theory and experiment for incompressible rubberlike solids *Proc. R. Soc. A Math. Phys. Eng. Sci.* **326** 565–84
- [27] Mosallaei M *et al* 2018 Geometry analysis in screen-printed stretchable interconnects *IEEE Trans. Components, Packag. Manuf. Technol.* **8** pp 1–1
- [28] Mosallaei M, Khorramdel B, Honkanen M, Iso-Ketola P, Vanhala J and Mantysalo M 2017 Fabrication and characterization of screen printed stretchable carbon interconnects 2017 IMAPS Nordic Conf. on Microelectronics Packaging (NordPac) pp 78–83
- [29] Mosallaei M, Jokinen J, Kanerva M and Mäntysalo M 2018 The effect of encapsulation geometry on the performance of stretchable interconnects *Micromachines* **9** 645